THE JOURNAL OF PHYSICAL CHEMISTRY C

Article

pubs.acs.org/JPCC

Lattice Dynamics Study of Nanocrystalline Yttrium Gallium Garnet at High Pressure

V. Monteseguro,[†] P. Rodríguez-Hernández,[†,‡] R. Vilaplana,[§] F. J. Manjón,[∥] V. Venkatramu,[⊥] D. Errandonea,[#] V. Lavín,[†,¶] and A. Muñoz*[,†,‡]

[†]Departamento de Física, and MALTA Consolider Team, Universidad de La Laguna. 38200 San Cristóbal de La Laguna, Santa Cruz de Tenerife, Spain

[‡]Instituto Universitario de Materiales y Nanotecnología, Universidad de La Laguna. 38205 San Cristóbal de La Laguna, Santa Cruz de Tenerife, Spain

[§]Centro de Tecnologías Físicas: Acústica, Materiales y Astrofísica, and MALTA Consolider Team, Universitat Politècnica de València, Cno. de Vera s/n, 46022 Valencia, Spain

[∥]Instituto de Diseño para la Fabricación y Producción Automatizada, and MALTA Consolider Team, Universitat Politècnica de València, Cno. de Vera s/n, 46022 Valencia, Spain

[⊥]Department of Physics, Yogi Vemana University, Kadapa-516 003, India

[#]Departamento de Física Aplicada-ICMUV, and MALTA Consolider Team, Universidad de Valencia, 46100 Burjassot (Valencia), Spain

[¶]Instituto Universitario de Estudios Avanzados en Atómica, Molecular y Fotónica, Universidad de La Laguna, 38205 San Cristóbal de La Laguna, Santa Cruz de Tenerife, Spain

ABSTRACT: This work reports an experimental and theoretical lattice dynamics study of nanocrystalline $Y_3Ga_5O_{12}$ (YGG) garnet at high pressures. Raman scattering measurements in nanocrystalline Tm^{3+}-doped YGG garnet performed up to 29 GPa have been compared to lattice dynamics ab initio calculations for bulk garnet carried out up to 89 GPa. Good agreement between the theoretical vibrational modes of bulk crystal and the experimental modes measured in the nanocrystals is found. The contribution of GaO_4 tetrahedra and GaO_6 octahedra to the different phonon modes of YGG is discussed on the basis of the calculated total and partial phonon density of states. Symmetries, frequencies, and pressure coefficients of the Raman-active modes are discussed. Moreover, the calculated infrared-active modes and their pressure dependence are reported. No pressure-induced phase transition has been observed in nano-YGG up to 29 GPa. This is in agreement with theoretical results, which show a mechanical instability of YGG above 84 GPa, similar to what occurs in $Gd_3Ga_5O_{12}$.

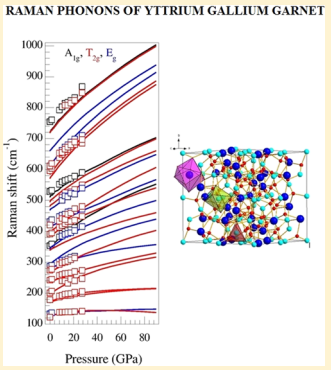

I. INTRODUCTION

In the last decades, oxide garnets and nanogarnets have been studied because of their importance in different technological applications. The combination of the great luminescence properties of rare earth (RE)-doped garnets and the hardness, high optical transparency, and mechanical and chemical stability of the garnet crystals makes them extremely useful as laser materials.[1,2] Moreover, the luminescence of Nd^{3+}-doped garnet crystals is used as pressure and/or temperature sensors for extreme condition experiments, as an alternative to ruby.[3] The interest in RE^{3+}-doped nanogarnets is based on the fact that the chemistry and optical spectroscopy of the analogous garnet bulk crystals are well-known, opening the possibility to establish meaningful comparisons between the properties of the nanosized and the bulk materials. In this sense, large efforts have been spent to investigate the luminescence properties of RE^{3+}-doped nanostructured garnets,[4] especially in the development of lasers and phosphors for lightning applications and as an alternative to quantum dots in the development of photonic and optoelectronic devices. Due to the numerous practical applications of garnets and nanogarnets, the understanding of their lattice dynamical properties is essential because phonons play an important role in the electrical, thermal, and optical properties of these materials. In this context, the lattice-dynamical properties of some garnets such as $Y_3Al_5O_{12}$ (YAG) and $Yb_3Al_5O_{12}$ (YbAG) have been studied both experimentally and theoretically at ambient pressure.[5]

$Y_3Ga_5O_{12}$ (YGG) garnet and nanogarnet can be considered as one of the oxide matrices with the lowest multiphonon relaxation probabilities providing a high quantum efficiency of the emitting levels of RE^{3+} ions. The knowledge of the lattice dynamics of YGG under pressure can help us understand the changes occurring in the solid-state properties of garnets and how this would affect the luminescence properties of the RE^{3+}

Received: February 13, 2014
Revised: May 22, 2014
Published: May 27, 2014

ions. High-pressure techniques offer a more powerful method for the study of the luminescence of rare earth ions, because applying pressure one can vary the interatomic distances and thereby obtain the crystal structure dependence of the f-electron states in RE^{3+} ions directly.[6] Despite the interesting properties and possible practical applications of YGG, to our knowledge, neither experimental nor theoretical studies of its lattice-dynamics properties at high pressures have been carried out. This is not the case of YAG, whose vibrational properties under pressure have been studied experimentally and theoretically.[7] In this respect, we have to note that theoretical studies, especially *ab initio* studies, of garnets under pressure are limited because of its high computational complexity because they involve many atoms in the primitive cell.[8,9]

YGG crystallizes in the body-centered cubic (bcc) structure (space group $Ia\bar{3}d$, No. 230, $Z = 8$) and has 160 atoms in the conventional unit cell (80 in the primitive cell). Two out of five Ga atoms of the formula unit occupy octahedral sites of S_6 symmetry (Wyckoff position 16a) whereas three out of five Ga atoms occupy tetrahedral sites of S_4 symmetry (Wyckoff position 24d). The three Y (or substitutional RE^{3+}) atoms occupy dodecahedral sites of D_2 symmetry (Wyckoff position 24c), and the 12 O anions occupy Wyckoff positions 96h that are characterized by three structural parameters (x, y, z).[10] In the garnet structure, each O atom is shared with one GaO_4 tetrahedron, one GaO_6 octahedron, and two YO_8 dodecahedra. Figure 1 shows the bcc structure of YGG with the three

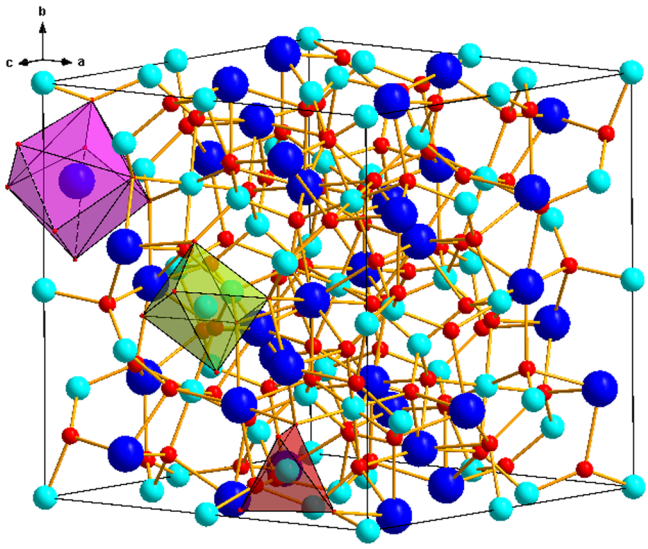

Figure 1. Unit cell of the $Y_3Ga_5O_{12}$ garnet structure. The YO_8 dodecahedron (violet), GaO_6 octahedron (green), and GaO_4 tetrahedron (red) polyhedra are highlighted. Big dark spheres (blue) represent the Y atoms, medium light spheres (blue) correspond to the Ga atoms, and the small dark (red) spheres correspond to the O.

mentioned polyhedra. At ambient conditions, typical theoretical internal parameters are $x = 0.1$, $y = 0.19408$, and $z = 0.27739$. Therefore, Y−O distances in YO_8 dodecahedra range from 2.34 to 2.42 Å, and the Ga(16a)−O and Ga(24d)−O distances are 1.99 and 1.84 Å in GaO_6 and GaO_4, respectively.[11]

In this paper we present an experimental and theoretical lattice dynamics study of the YGG garnet and nanogarnet. We report Raman scattering measurements in nanocrystalline Tm^{3+}-doped YGG garnet, synthesized by the citrate sol−gel method, up to 29 GPa, and lattice dynamics *ab initio* calculations for bulk garnet up to 89 GPa. Symmetries, frequencies, and pressure coefficients of the experimental and calculated Raman-active modes are discussed. The calculated infrared-active modes and their pressure dependence are also reported. The phonon modes of YGG will be discussed in relation to the internal and external molecular modes of the different polyhedra on the basis of the calculated total and partial phonon density of states. No pressure-induced phase transition has been observed up to 29 GPa. This result is in good agreement with our theoretical study which predict that the YGG garnet is mechanically unstable above 84 GPa.[11]

II. AB INITIO CALCULATIONS

Ab initio total-energy calculations have been performed within the framework of the density functional theory (DFT).[12] The VASP package has been used to carry out calculations with the pseudopotential method and the projector augmented wave scheme (PAW).[13] We employ ultrasoft pseudopotentials, which replace the core electrons and make smoothed pseudovalence wave functions. For yttrium, 11 valence electrons are used ($4s^24p^65s^24d^1$), whereas 13 valence electrons ($3d^{10}4s^24p^1$) are used for gallium and 6 valence electrons ($2s^22p^4$) are used for oxygen. Highly converged results were achieved by extending the set of plane waves up to a kinetic energy cutoff of 520 eV. The exchange−correlation energy was taken in the generalized gradient approximation (GGA) with the PBEsol[14] prescription. A dense Monkhorst−Pack grid of k-special points was used to perform integrations along the Brillouin zone (BZ) to obtain very well converged energies and forces. At each selected volume, the structures were fully relaxed to their equilibrium configuration through the calculation of the forces on atoms and the stress tensor. In this relaxation, only oxygen ions reorganize to look for such equilibrium structure because these ions depend on three internal structural parameters, whereas yttrium and gallium ions occupy high-symmetry Wyckoff positions. In the relaxed configurations, the forces on the atoms are less than 0.006 eV/Å and deviations of the stress tensor from a diagonal hydrostatic form are less than 0.1 GPa.

It is useful to note that the theoretical pressure, $P(V)$, can be obtained within the DFT formalism at the same time as the total energy, $E(V)$. The theoretical pressure, P, like other derivatives of the energy, is obtained from the calculated stress.[15]

Lattice-dynamics calculations were performed at the zone center (Γ point) of the BZ. Highly converged results on forces are required for the calculation of the dynamical matrix using the direct force constant approach.[16] The construction of the dynamical matrix at the Γ point of the BZ involves separate calculations of the forces in which a fixed displacement from the equilibrium configuration of the atoms within the primitive cell is considered. The number of such independent displacements in the analyzed structures is reduced due to the crystal symmetry. Diagonalization of the dynamical matrix provides the frequencies of the normal modes. Moreover, these calculations allow identifying the symmetry and eigenvectors of the vibrational modes in each structure at the Γ point.

III. EXPERIMENTAL DETAILS

Nanocrystalline $Y_{3(1-x)}Tm_{3x}Ga_5O_{12}$ yttrium−gallium garnet doped with thulium ions ($x = 0.01$) was synthesized by the citrate sol−gel method in air atmosphere.[17] Stoichiometric molar ratios of high-purity $Ga(NO_3)_3{\cdot}9H_2O$, $Y(NO_3)_3{\cdot}4H_2O$,

dx.doi.org/10.1021/jp501570c | J. Phys. Chem. C 2014, 118, 13177−13185

and $Tm(NO_3)_3{\cdot}5H_2O$ materials were dissolved in 25 mL of 1 M HNO_3 under stirring at 353 K for 3 h. Then citric acid, with a molar ratio of metal ions to citric acid of 1:2, was added to the solution, which was stirred for 2 h more and finally dried at 363 K for 36 h. This process created a gel that was fired at 773 K for 4 h to remove the residual nitrates and organic compounds and the subsequently obtained powder sample was finally calcined at 1173 K for 16 h. The structure of the YGG nanogarnet at ambient pressure was checked by X-ray diffraction using the Cu $K\alpha_1$ (1.5406 Å) radiation in the range $2\theta = 10-80°$, with a step size of 0.020 (PANalytical X'Pert Pro). The XRD pattern of YGG nanogarnet under study can be identified with the cubic structure and the average crystallite size was estimated to be around 60 nm from the full width at half-maximum (fwhm) of the diffraction peak at 32.71° using the Scherrer equation, confirming the estimations made using HRTEM micrographs.[18] The unit cell parameter for the YGG nanogarnet under study is 12.28 Å, which compares with the experimental data of bulk YGG (12.273 Å)[19] and with the calculated value 12.278 Å.[11] This result suggests that, at least from the structural point of view, our nanogarnets should behave as bulk material. We will show along this paper that the same applies for the vibrational properties.

The prepared nanopowder sample of YGG, along with a 2-μm-diameter ruby ball, was loaded in a preindented tungsten gasket with a 150-μm-diameter hole inside a diamond-anvil cell. A 16:3:1 methanol−ethanol−water mixture was used as the pressure-transmitting medium,[20] and the pressure was determined by monitoring the shift in ruby fluorescence lines.[21] The 16:3:1 methanol−ethanol−water mixture behaves hydrostatically up to 10.5 GPa and quasi-hydrostatically up to the maximum pressure attained in this study (29 GPa).[20,22] High-pressure Raman scattering measurements were performed in backscattering geometry using a 632.8 nm HeNe laser and a microspectrometer (Horiba-JobinYvon LabRAM HR UV) in combination with a thermoelectrically cooled multichannel CCD detector with spectral resolution below 2 cm^{-1}. Experimental frequencies of the Raman modes were obtained by fitting peaks with a Voigt profile (Lorentzian convoluted with a Gaussian) after proper calibration and background subtraction of the experimental spectra. The Gaussian line width was fixed to the experimental setup resolution to get the three variables of the Lorentzian profile for each peak.

IV. RESULTS AND DISCUSSION

A. Lattice Dynamics of YGG at Ambient Pressure. According to group theoretical considerations, the $Ia\bar{3}d$ structure of the YGG has 98 vibrational modes that can be classified at the BZ center as 25 Raman-active modes (Γ_R), 17 infrared-active modes (Γ_{IR}), 55 optically inactive (silent) modes (Γ_S), and 1 acoustic (T_{1u}) mode,

$$\Gamma_R = 3A_{1g} + 8E_g + 14T_{2g}$$

$$\Gamma_{IR} = 17T_{1u}$$

$$\Gamma_S = 16T_{2u} + 14T_{1g} + 5A_{2u} + 5A_{2g} + 10E_u + 5A_{1u}$$

where E and T (also noted F in the literature) modes are doubly and triply degenerated, respectively.

The Raman scattering spectrum of our Tm^{3+}-doped YGG nanocrystal at ambient condition is shown in Figure 2. It is compared to those of bulk YGG garnet and pure YGG nanocrystal. As can be seen, all three Raman spectra are similar;

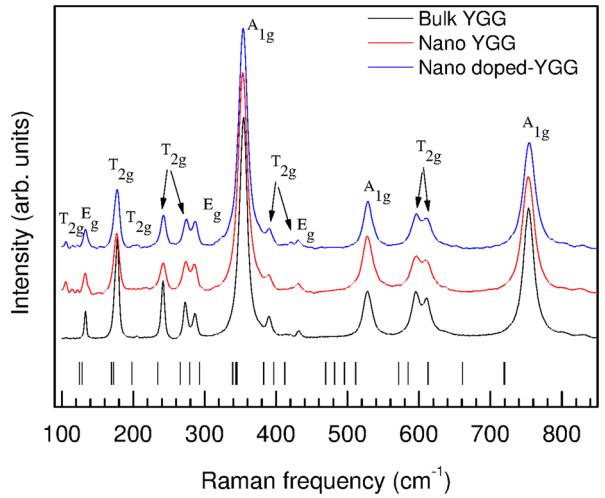

Figure 2. Experimental Raman spectra of the bulk $Y_3Ga_5O_{12}$ garnet, nanogarnet, and Tm^{3+}-doped nanogarnet at ambient conditions. Bottom vertical ticks indicate the *ab initio* frequencies of the Raman active modes.

showing the same frequencies and linewidths within experimental error. The similarity of the Tm^{3+}-doped YGG and the pure YGG nanogarnet evidence that 1% Tm doping does not have any effect in the vibrational properties of YGG nanocrystals. On the other hand, the similarity of the Tm^{3+}-doped YGG nanocrystal and the pure bulk YGG evidence that 60 nm size YGG nanogarnets show the same vibrational properties of bulk YGG, as expected because of the similar lattice parameters previously commented.

Only 17 out of the 25 Raman-active modes theoretically predicted have been measured. In this respect, it is likely that some modes are too weak to be observed and there is an accidental degeneracy of several modes at room pressure. At the bottom of Figure 2, vertical marks represent the theoretical frequencies of the Raman-active modes predicted at ambient conditions to directly compare with the experimental spectra. The experimental and theoretical frequencies of the Raman-active modes at ambient pressure are summarized in Table 1. The Raman spectrum can be divided into two regions: the low-frequency region (100−550 cm^{-1}) and the high-frequency region (550−800 cm^{-1}). This division contrasts with that of the Raman spectrum of YAG, which has three regions (see refs 7 and 23). This can be understood if one considers that gallium garnets have a larger unit cell volume than that of aluminum garnets, and besides, the gallium has a mass greater than the aluminum. Consequently, there is a red shift in the high-frequency modes of gallium garnets with respect to aluminum garnets, which results in an overlapping of the high and intermediate regions in the Raman spectrum of the YGG.

Figure 2 also shows the tentatively assigned symmetries of the observed modes on the basis of our theoretical calculations and on the comparison with previous works of lattice dynamics in garnets. There is a quite good agreement between the theoretical frequencies of the vibrational modes of bulk crystal and the experimental modes measured in the nanocrystals with average sizes of 60 nm (Table 1). In general, only slight shifts in frequency have been found; they are likely due to the GGA approximation, which tends to underestimate the frequencies.

Till now, the Raman spectrum of garnets has been usually interpreted by assuming that the different Raman modes could be attributed to the vibrational modes of the tetrahedral

dx.doi.org/10.1021/jp501570c | J. Phys. Chem. C 2014, 118, 13177−13185

Table 1. Theoretical and Experimental Frequencies, Pressure Coefficients, and Zero-Pressure Grüneisen Parameters for the Raman-Active Modes of the YGG[a]

	ab initio				experimental			
Raman mode symmetry	ω_0 (cm^{-1})	$\partial\omega/\partial P$ (cm^{-1}/GPa)	$\partial^2\omega/\partial P^2$ (cm^{-1}/GPa^2)	γ	ω_0 (cm^{-1})	$\partial\omega/\partial P$ (cm^{-1}/GPa)	$\partial^2\omega/\partial P^2$ (cm^{-1}/GPa^2)	γ
T_{2g}	124.5	0.74	−0.007	1.00	122.4	1.72	−0.042	2.37
E_g	128.4	0.43	−0.003	0.56	133.3[b]			
T_{2g}	169.6	0.96	−0.006	0.95	187.5[c]	1.09	−0.013	0.98
T_{2g}	172.3	1.13	−0.008	1.11	178.6	1.62	−0.024	1.53
T_{2g}	198.1	2.31	−0.012	1.97	200.8	3.75	−0.084	3.15
T_{2g}	234.1	1.52	−0.006	1.09	242.2	1.93	−0.03	1.34
T_{2g}	265.9	2.15	−0.007	1.36	274.1	2.46	−0.028	1.51
E_g	278.9	1.54	−0.008	0.93	286.9	1.91	−0.019	1.12
E_g	292.7	2.6	−0.012	1.49	359.8[f]			
T_{2g}	339.1	1.93	−0.007	0.96				
A_{1g}	343.4	3.47	−0.014	1.70	353.8	4.26	−0.08	2.03
E_g	345.2	2.58	−0.01	1.26	384.7[d]	0.82	0.025	0.36
T_{2g}	382.5	2.53	−0.009	1.11	391.1	3.04	−0.036	1.31
T_{2g}	396.5	2.95	−0.007	1.25	420.5	1.93	0.017	0.77
E_g	412.2	1.95	−0.003	0.79	431.2	2.39	−0.034	0.93
E_g	469.3	2.51	−0.006	0.90	500.0[d]	2.4	−0.009	0.81
T_{2g}	481.8	2.64	−0.008	0.92	510.0[d]	2.39	−0.007	0.79
T_{2g}	495.6	2.93	−0.008	0.99				
A_{1g}	511.4	2.79	−0.008	0.92	528.4	3.22	−0.03	1.02
T_{2g}	571.8	4.64	−0.015	1.37	595.8	6.32	−0.11	1.78
T_{2g}	584.9	4.59	−0.015	1.32	611.5	5.19	−0.07	1.43
E_g	612.7	4.61	−0.015	1.27	661.8[d]	5.90	−0.08	1.50
E_g	661.1	4.18	−0.013	1.07	776.4[f]			
T_{2g}	719.2	4.23	−0.013	0.99	807.8[e]	4.02	−0.03	0.89
A_{1g}	719.9	4.27	−0.014	0.99	754.8	4.24	−0.01	0.94

[a]The pressure dependence of both experimental and theoretical frequencies has been fitted with a second-order polynomial: $\omega = \omega_o + (\partial\omega/\partial P)P + (\partial^2\omega/\partial P^2)P^2$ up to 29 and 89 GPa, respectively. [b]This mode only appears at 0 GPa. [c]This mode appears above 8 GPa. [d]These modes appear above 10 GPa. [e]This mode appears above 13 GPa. [f]These modes appear above 25 GPa, with the values indicated in the table.

(GaO_4), octahedral (GaO_6), and dodecahedral (YO_8) units. However, the attribution of each Raman mode to a single unit is not straightforward because the vibrations of the different polyhedra are strongly coupled to each other. Therefore, to understand the contribution of each polyhedral unit to every Raman mode, we have calculated both the total and the partial (or projected onto each atom) phonon density of states (Figure 3), so that the dynamical contribution of each atom can be observed. It can be noted that Ga atoms with octahedral coordination (Ga_{oct}) predominantly contribute in the low-frequency region, especially between 200 and 300 cm^{-1}, and with a small contribution in the high-frequency region. Ga atoms with tetrahedral coordination (Ga_{tet}) have the greatest contribution in the low-frequency region, mainly between 100 and 200 cm^{-1}. On the other hand, Ga atoms with tetrahedral coordination are the Ga atoms that contribute in the high-frequency region. O atoms contribute in both the low- and high-frequency regions, its main contribution being above 260 cm^{-1}. Finally, Y atoms contribute in the low-frequency region between 100 and 400 cm^{-1} with special intensity in the region between 100 and 200 cm^{-1}. As a result, the RE^{3+} ions, which substitute the Y ones in the dodecahedral site, show low multiphonon relaxation probabilities, thus favoring the spontaneous emission of photons when the RE^{3+} ions are excited. This is the origin of the high quantum yield of luminescence of the RE^{3+} ions in the garnet and nanogarnet structures.[18]

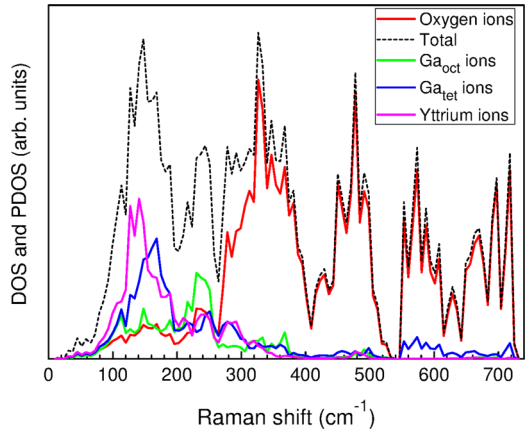

Figure 3. Partial and total phonon density of states of the $Y_3Ga_5O_{12}$ garnet. The total phonon density is the dotted black curve.

On the basis of the contributions of the individual atoms we can now discuss the contributions of the different polyhedra to each vibrational mode. According to Hurrel et al.,[24] the phonon modes of a garnet crystal with general formula $P_3Q_2(RO_4)_3$, with P, Q, and R being cations, are a combination of the molecular modes of the RO_4 and QO_6 polyhedra. This view has been further used to describe the phonon modes of aluminate[5] and silicate[25] garnets. Due to the structural similarity of aluminum garnets and gallium garnets, the internal Raman-active modes of YGG could be assigned in a similar way as those for YAG.[5,23,24] The most intense Raman modes of YGG correspond to the three A_{1g} modes (Figure 2). These three

dx.doi.org/10.1021/jp501570c | J. Phys. Chem. C 2014, 118, 13177−13185

modes are directly connected with the free GaO_4 and GaO_6 internal vibrations: the higher frequency A_{1g} mode must correspond to the symmetric stretching mode of tetrahedra and octahedra in antiphase to each other; the intermediate A_{1g} mode might be related with the bending mode of tetrahedra and octahedra; and finally, the lower frequency A_{1g} mode can be assigned to the rotational mode of octahedra and a small contribution of the rotational mode of tetrahedra.

In the high-frequency region, the last E_g mode at 661 cm^{-1} corresponds to symmetric stretching mode of GaO_4 and antisymmetric stretching mode of GaO_6, whereas the last T_{2g} mode at 719 cm^{-1} corresponds to the symmetric stretching mode of the tetrahedra and octahedra.

In the low-frequency region, translational movements of the GaO_4 and YO_8 can be observed. The first T_{2g} mode at 124 cm^{-1} and the first E_g mode at 128 cm^{-1} correspond to translational movements of these two polyhedral, although the E_g mode has a greater translation of the dodecahedra. The following four T_{2g} modes at 169, 172, 198, and 234 cm^{-1} are mainly related with translational movements of the tetrahedra. Apparently, there is not a translational movement of the YO_8 unit in these modes, only a translational movement of the Y cations. The E_g and T_{2g} modes, with frequencies of 345 and 382 cm^{-1}, respectively, might be related with the rotational mode of GaO_4 tetrahedra and GaO_6 octahedra. The E_g mode at 469 cm^{-1} and the two T_{2g} modes with frequencies 481 and 495 cm^{-1} are assigned to symmetric bending modes of GaO_4 and GaO_6. For the rest of the vibrational modes, our calculations suggest a complex vibrational pattern so it is not easy to distinguish the contributions of the different polyhedra.

It is important to note that our theoretical results do not predict the existence of Raman-active modes below 100 cm^{-1}. This result is confirmed by our Raman scattering measurements and it can be explained by the dense structure of YGG and the strong atomic interactions between the different polyhedra. These strong atomic interactions also account for the complexity of the vibrational pattern of garnets and the difficulty of explaining their vibrational modes in terms of the isolated polyhedral units.[5]

B. Lattice Dynamics of YGG at High Pressures. Selected experimental Raman spectra of nanocrystalline Tm^{3+}-doped YGG at different pressures up to 27 GPa are shown in Figure 4. As can be observed, all phonon frequencies exhibit a monotonous increase with pressure due to the contraction of the interatomic distances in the unit-cell volume. As already commented, only 17 Raman-active modes are visible at room pressure; however, as the pressure increases, there is a rupture of the degeneracy of some peaks such as the mode T_{2g} at 187.5 cm^{-1} from 8 GPa, the mode E_g at 384 cm^{-1} and at 661.85 cm^{-1} from 10 GPa, and the last mode T_{2g} at 807.8 cm^{-1} from 13 GPa. Moreover, and as can be seen in Figure 4, the intensity of other Raman modes increases with the pressure and they can be observed in the Raman spectrum. The intensities of the modes E_g (500 cm^{-1}) and T_{2g} (510 cm^{-1}) increase from 10 GPa whereas the modes E_g at 359.78 and 776.37 cm^{-1} appear above 25 GPa. Therefore, and according to the evolution of Raman modes with the pressure observed in Figure 4, the bcc structure is stable up to 29 GPa.

The pressure dependences of the experimental and theoretical Raman-active mode frequencies up to 29 and 89 GPa, respectively, are shown in Figure 5. These frequencies are similar within 5% of accuracy as can be observed in the pressure coefficients of the Raman-active modes in Table 1. This good

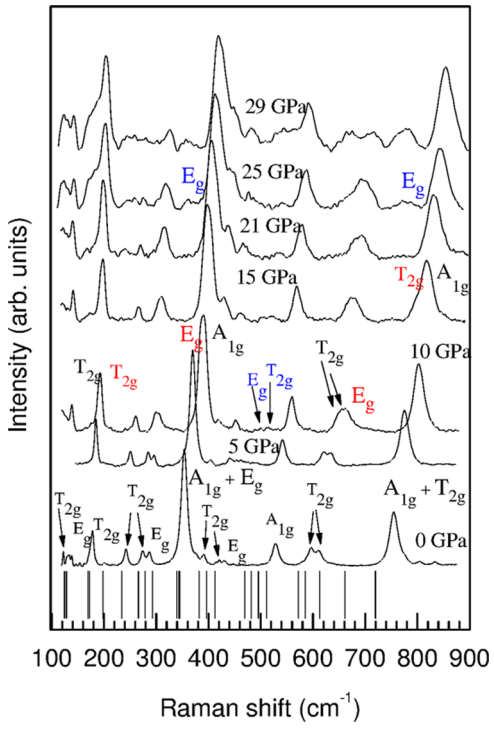

Figure 4. Experimental Raman spectra at pressures between 0 and 29 GPa of the Tm^{3+}-doped $Y_3Ga_5O_{12}$ nanogarnet. Additional modes that appear due to the rupture of degeneracy are shown in red letters; the modes represented with blue letters increase their intensity.

agreement between the experimental and theoretical modes reflects (i) that the introduction of RE^{3+} ions in the nanogarnet up to a concentration of 1% mol does not change the lattice dynamics of the material and (ii) that the vibrational properties of our nanogarnets are quite similar to those of the bulk garnet.

It is worth noting that all modes show a positive first-order pressure coefficient. Only the lowest frequency phonon modes (T_{2g} and E_g modes) show a very small pressure coefficient (Table 1), indicating that these modes have very low volume dependence. For completeness, we present in Table 2 the IR-active mode frequencies (TO component) at ambient pressure and their pressure coefficients. Our values for the IR-active mode frequencies at ambient pressure can be found in good agreement with those reported for bulk YGG (Table 2).[26]

As can be observed in Figures 5 and 6, the first T_{2g} Raman mode and the three first T_{1u} infrared modes decrease at high pressure, which suggests a possible pressure-induced instability.[27] This instability is reflected in the lowest frequency silent T_{2u} mode (Figure 7) that becomes negative at 111 GPa. Therefore, this result is in agreement with a previous theoretical study, where it was shown that YGG becomes mechanically unstable above 84 GPa,[11] and with other experimental results of gallium garnets, such as $Gd_3Sc_2Ga_3O_{12}$ (GSGG) and $Gd_3Ga_5O_{12}$ (GGG), which have a pressure-induced amorphization at 58 ± 3 and 84 ± 4 GPa, respectively.[28] Experimentally, a considerable broadening of Raman peaks with increasing pressure is observed, although no pressure-induced phase transition has been noted up to 27 GPa (Figure 4).

Both experimental and theoretical Grüneisen parameters, $\gamma = (B/\omega)(\partial\omega/\partial P)$, are compared in Table 1. They have been estimated by using the theoretical value for the bulk modulus, B_0 = 168.54 GPa, calculated from the fourth-order Birch–Murnaghan equation of state.[29] This bulk modulus is similar to

dx.doi.org/10.1021/jp501570c | J. Phys. Chem. C 2014, 118, 13177−13185

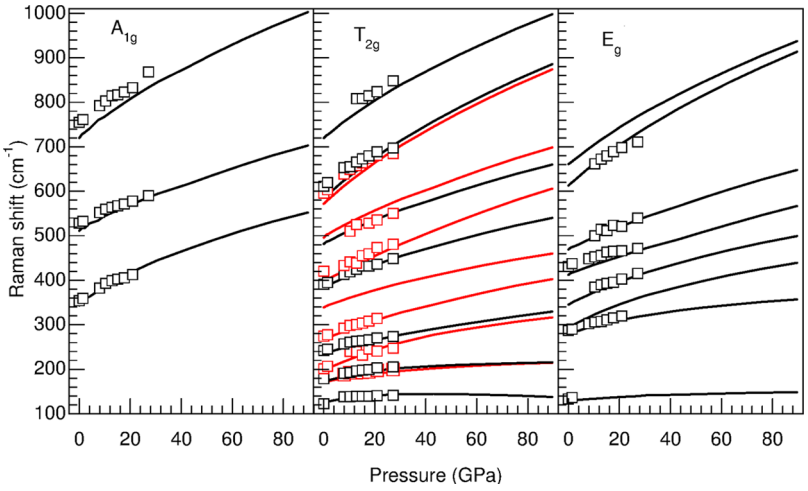

Figure 5. Theoretical and experimental pressure dependence of the A_{1g}, T_{2g}, and E_g Raman modes of the $Y_3Ga_5O_{12}$ garnet. Lines represent the *ab initio* calculated frequencies and empty squares represent the experimentally observed frequencies. The colors, red and black, in the modes T_{2g} are only used as a guideline for the eyes.

Table 2. Theoretical Frequencies, Pressure Coefficients, and Grüneisen Parameters for the Infrared-Active Modes of Bulk YGG at Ambient Pressure[a]

experimental data[b]	theoretical data			
ω_0 (cm^{-1})	ω_0 (cm^{-1})	$\partial\omega/\partial P$ (cm^{-1}/GPa)	$\partial^2\omega/\partial P^2$ (cm^{-1}/GPa^2)	γ
107.8	101.7	0.39	−0.009	0.65
113.1	107.4	0.35	−0.006	0.55
147.3	140.3	0.55	−0.007	0.66
157.8	153.6	0.78	−0.005	0.86
202	193.1	0.57	−0.005	0.49
235.2	228.7	1.36	−0.008	1.00
258	249.5	2.21	−0.011	1.49
304.8	294.6	2.15	−0.009	1.23
317.5	313.9	1.86	−0.006	0.99
328.8	317.2	1.84	−0.005	0.98
370.3	359.9	2.31	−0.008	1.08
374.3	362.7	3.48	−0.01	1.62
420	405.3	2.80	−0.005	1.16
479	461.1	2.89	−0.007	1.06
588.4	564.2	4.79	−0.016	1.43
621.7	597.5	4.61	−0.014	1.30
688.4	659.9	4.48	−0.014	1.14

[a]The pressure dependence of theoretical frequencies has been fitted with a second-order polynomial: $\omega = \omega_o + (\partial\omega/\partial P)P + (\partial^2\omega/\partial P^2)P^2$. [b]Experimental data for bulk YGG from ref 26 is added for comparison.

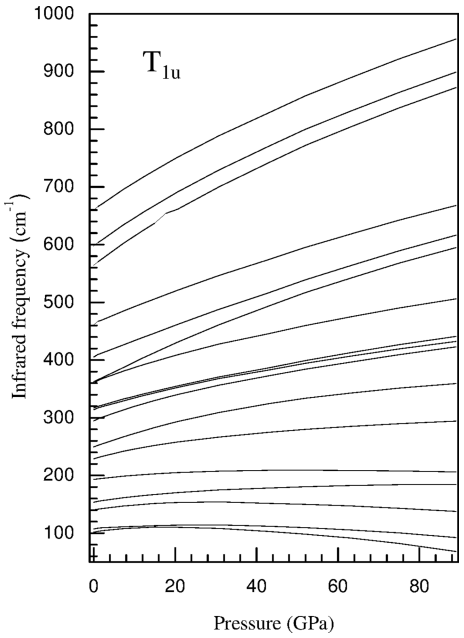

Figure 6. Calculated pressure evolution of the 17 T_{1u} infrared modes of the $Y_3Ga_5O_{12}$ garnet.

those of most garnets (between 150 and 180 GPa).[30] The theoretical (experimental) Grüneisen parameter has a greater variation in the low-frequency region, where γ ranges from 0.56 (0.36) to 1.97 (3.15), than in the high-frequency region, where it ranges from 0.99 (0.79) to 1.37 (1.70). Therefore, there are larger differences in the restoring forces on the atoms of polyhedra related to the lowest modes. The lowest E_g mode (mode assigned to the translation of the YO_8 unit) has a very small pressure coefficient and Grüneisen parameter at ambient pressure, indicating that the restoring force between YO_8 decreases as the pressure increases. Theoretical Grüneisen parameters of infrared modes vary between 1.49 and 0.49. The five lowest frequency IR modes have the lowest Grüneisen parameters; suggesting that the restoring forces between the atoms of the different polyhedra are weaker at higher pressures.

It is interesting to compare the pressure dependence of the Raman modes of YGG with those reported for YAG in ref 7. It can be observed that the six highest frequency modes, which correspond to the high-frequency region in both compounds, and which can be associated with internal vibrations of the AlO_4 (AlO_6) and GaO_4 (GaO_6) tetrahedra (octahedra) in YAG and YGG, respectively, show the highest pressure coefficients, which in turn are similar in both YAG and YGG. This result indicates a similar pressure dependence of the Al−O and Ga−O bonds in the tetrahedra and octahedra, which are the most incompressible units. The comparison in the low-frequency regions below 560 cm^{-1} in both compounds is much more difficult because the modes in YGG are much closer between them than in YAG. However, it must be mentioned that the A_{1g} mode of lowest frequency shows a much larger pressure

dx.doi.org/10.1021/jp501570c | J. Phys. Chem. C 2014, 118, 13177−13185

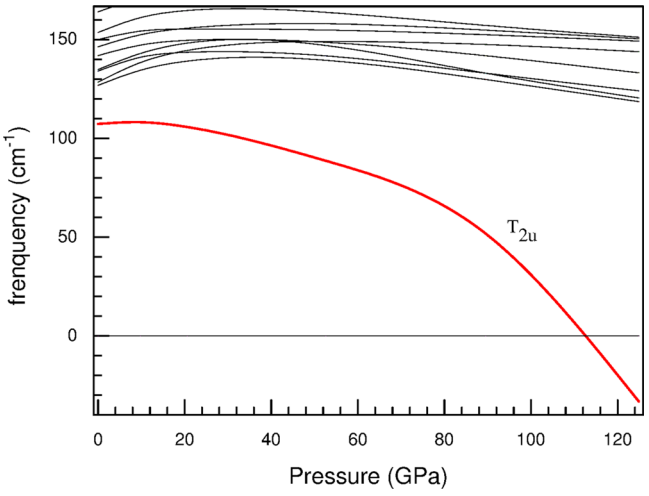

Figure 7. Theoretical pressure dependence of the first T_{2u}, A_{1u}, T_{1g}, A_{2g}, and E_u silent modes of the $Y_3Ga_5O_{12}$ garnet.

coefficient in YGG (4.26 cm^{-1}/GPa) than in YAG (1.7 cm^{-1}/GPa). On the other hand, it must be noted that the lowest frequency T_{2g} mode, which is related to a translation of the YO_8 dodecahedra, shows similar Grüneisen parameters in both compounds. This indicates that the rates of hardening of bonds related to this translation with pressure are similar in YGG and YAG, despite the different compressibility considered for both compounds, B_0(YGG) = 168.5 GPa and B_0(YAG) = 185.2 GPa.[7]

In a previous work on RE^{3+}-doped garnets, Papagelis et al. mentioned that in the garnet series only RE^{3+}−O distances, and consequently Y−O distances, vary significantly when the crystal volume decreases.[23] Figure 8 shows the theoretical pressure dependence of different interatomic distances in YGG. It can be observed how all distances decrease with increasing pressure, in good agreement with the increase of the Raman frequencies.

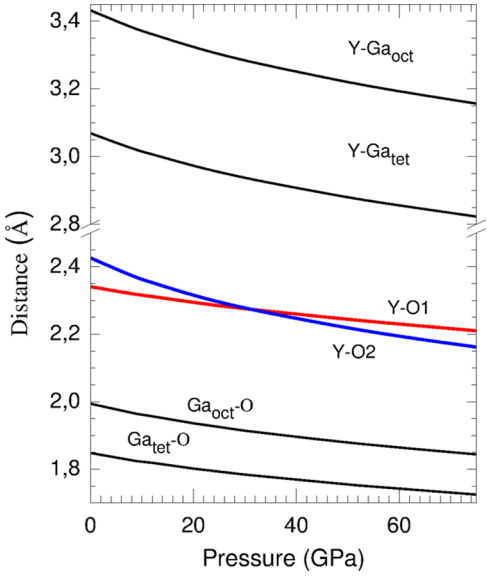

Figure 8. Evolution of the interatomic distances as a function of the pressure of the $Y_3Ga_5O_{12}$ garnet. Ga_{tet} stands for Ga atoms with tetrahedral coordination, Ga_{oct} stands for Ga atoms in octahedral coordination. Y−O1 and Y−O2 are the smallest and largest Y−O distances in the irregular YO_8 dodecahedra.

Our calculations indicate that in the coordination polyhedra one of the distances between the yttrium ions and the oxygen ions, Y−O1, changes at a rate of -2×10^{-3} Å/GPa, whereas the Y−O2 distance varies faster, about -5.6×10^{-3} Å/GPa. Therefore, the YO_8 dodecahedra are quite irregular at low and high pressures.

Moreover, the similar decrease of the Y−Ga_{tet} and Y−Ga_{oct} distances (with a rate of -5×10^{-3} Å/GPa) on increasing pressure indicates that the influence between dodecahedra and tetrahedra or octahedra is similar in the full pressure range up to 89 GPa. Curiously, the larger contraction of distances related to Y is not reflected in larger pressure coefficients for the modes related to Y between 100 and 200 cm^{-1}. On the contrary, the three Raman-active modes and the five IR-active modes with the smallest frequencies show the smallest Grüneisen parameters. This result evidences a strong decrease of the force constant between Y and O atoms in YO_8 dodecahedra with increasing pressure that compensates the strong decrease of the Y−O2 bond distance and it confirms that GaO_4 and GaO_6 polyhedra are the basic units of the gallium garnet also at high pressures.

Finally, it is worth noting that the decrease of the Y−O2 bond force constant must be related to a charge transfer to any of the Ga−O bonds. This transfer should lead to a larger pressure coefficient of vibrational modes related to these Ga−O bonds. In this respect, it is noteworthy that the modes with the largest pressure coefficients are those with frequencies above 550 cm^{-1} that are related to Ga_{tet} and Ga_{oct}, as suggested by Figure 3. This result indicates that on increasing pressure there is an increase of the charge transfer mainly from Y−O2 bonds to Ga−O bonds in GaO_4 tetrahedra and GaO_6 octahedra. This makes sense, because O2 atoms correspond to those of the tetrahedral and octahedra.

V. CONCLUSIONS

We have carried out an experimental and theoretical lattice dynamics study of YGG nanogarnet under high pressure by performing Raman scattering measurements in nanocrystalline Tm^{3+}-doped YGG garnet up to 27 GPa and *ab initio* calculations of bulk YGG up to 89 GPa. Theory predicts 25 Raman-active modes, 17 infrared-active modes, whose pressure dependences have been reported, and 55 optically inactive (silent) modes. The results of the Raman scattering measurements in the nanogarnet with sizes of around 60 nm are in good agreement with the theoretical results in bulk garnet. The agreement between the experimental and theoretical frequencies shows that the introduction of a RE^{3+} in the nanogarnet, up to 1% concentration, does not change the lattice dynamics of the material and that the vibrational properties of our nanogarnets are similar to those of the bulk garnet.

To discuss the contribution of each atom to the different Raman vibrational modes, we have analyzed the total and the partial phonon density of states that reflects the dynamical contribution of each atom. Y (or possible substituting RE^{3+}) and octahedrally coordinated Ga atoms mainly contribute in the low-frequency region whereas the tetrahedrally coordinated Ga and O atoms contribute in both low- and high-frequency regions. Furthermore, the Raman phonon modes of the YGG crystal have associated internal and external molecular modes of the different polyhedra. In the low-frequency regions, 124−234 and 345−382 cm^{-1}, the translational modes of YO_8 and GaO_4 and the rotational modes of GaO_4 and GaO_6, respectively, dominate in the Raman spectrum. In the high-frequency

dx.doi.org/10.1021/jp501570c | J. Phys. Chem. C 2014, 118, 13177−13185

regions, 469−500 and 661−719 cm^{-1}, the internal modes of GaO_6 and GaO_4 polyhedra, such as bending and stretching modes respectively, are present in the YGG.

Finally, we want to comment that experimentally no pressure-induced phase transition upon pressure up to 27 GPa has been observed, as expected, in the nanogarnets. However, several Raman, IR, and silent modes decrease with increasing pressure, thus suggesting a pressure-induced instability. These results are in agreement with previous calculations that showed that the YGG garnet structure becomes mechanically unstable above 84 GPa.[11]

AUTHOR INFORMATION

Corresponding Author

*A. Muñoz: e-mail, amunoz@ull.edu.es; phone, +34 922318275.

Notes

The authors declare no competing financial interest.

ACKNOWLEDGMENTS

This work has been supported by Ministerio de Ciencia e Innovación of Spain (MICINN) under the National Program of Materials (MAT2010-21270-C04-01/02/03/04) and the Consolider-Ingenio 2010 Program (MALTA CSD2007-0045) and by the EU-FEDER funds. V. Monteseguro, V. Lavín, and V. Venkatramu are also grateful to MINECO from Spain and Department of Science and Technology of India for financial support within the Indo-Spanish Joint Programme of Cooperation in Science and Technology (DST-INT-Spain-P-38-11/PRI-PIBIN-2011-1153). V. Monteseguro thanks MICINN for the FPI grant (BES-2011-044596). R. Vilaplana and F. J. Manjón acknowledge financial support from Generalitat Valenciana through project GVA-ACOMP-2013-012 and by the Vicerrectorado de Investigación y Desarrollo of the Universitat Politècnica de València through projects UPV2011-0914 PAID-05-11 and UPV2011-0966 PAID-06-11. V. Venkatramu is grateful to Council of Scientific and Industrial Research (CSIR, New Delhi) for the sanction of major research project (No. 03(1229)/12/EMR-II, dated 16th April, 2012).

REFERENCES

(1) Morrison, C. A.; Leavitt, R. P. Spectroscopic properties of triply ionized lanthanides in transparent host crystals. In *Handbook of the Physics and Chemistry of Rare Earths*; Gschneidner, K. A., Jr., Eyring, L., Eds.; North Holland Publishing Company: Amsterdam, 1982; Vol. *5*, Chapter 46, pp 461−701.

(2) Speghini, A.; Piccinelli, F.; Bettinelli, M. Synthesis, Characterization and Luminescence Spectroscopy of Oxide Nanopowders Activated with Trivalent Lanthanide Ions: The Garnet Family. *M. Opt. Mater.* **2011**, *33*, 247−257.

(3) Rodríguez-Mendoza, U. R.; León-Luis, S. F.; Muñoz-Santiuste, J. E.; Jaque, D.; Lavín, V. Nd^{3+}-doped $Ca^3Ga^2Ge^3O_{12}$ Garnet: A New Optical Pressure Sensor. *J. Appl. Phys.* **2013**, *113*, 213517-1−8.

(4) Venkatramu, V.; Giarola, M.; Mariotto, G.; Polizzi, S.; Jayasankar, C. K.; Piccinelli, F.; Bettinelli, M.; Speghini, A. Nanocrystalline Lanthanide-Doped $Lu_3Ga_5O_{12}$ Garnets: Interesting Materials for Light-Emitting Devices. *Nanotechnology* **2010**, *21*, 175703−175712.

(5) Papagelis, K.; Kanellis, G.; Ves, S.; Kourouklis, G. A. Lattice Dynamical Properties of the Rare Earth Aluminum Garnets ($RE_3Al_5O_{12}$). *Phys. Status Solidi B* **2002**, *233*, 134−150.

(6) Tröster, Th. Optical studies of non-metallic compounds under pressure. In *Handbook of the Physics and Chemistry of Rare Earths*; Gschneidner, K. A., Jr., Bünzli, J.-C. G., Pecharsky, V. K., Eds.; Elsevier Science B. V.: Amsterdam, 2003; Vol. *33*, Chapter 217, pp 515−589.

(7) Arvanitidis, J.; Papagelis, K.; Christofilos, D.; Kimura, H.; Kourouklis, G. A.; Ves, S. High Pressure Raman Study of $Y_3Al_5O_{12}$. *Phys. Status Solidi B* **2004**, *241*, 3149−3154.

(8) Guo, H.; Zhang, M.; Han, J.; Zhang, H.; Song, N. First Principles Study of Structural, Phonon, Optical, Elastic and Electronic Properties of $Y_3Al_5O_{12}$. *Physica B* **2012**, *407*, 2262−2266.

(9) Goel, P.; Mittal, R.; Choudhury, N.; Chaplot, S. L. Lattice Dynamics and Born Instability in Yttrium Aluminum Garnet, $Y_3A1_5O_{12}$. *J. Phys.: Condens. Matter* **2010**, *22*, 065401 1−11..

(10) Nakatsuka, A.; Yoshiasa, A.; Takeno, S. Site Preference of Cations and Structural Variation in $Y_3Fe_{5-x}Ga_xO_{12}$ ($0 \le x \le 5$) Solid Solutions with Garnet Structure. *Acta Crystallogr.* **1995**, *B51*, 737−745.

(11) Monteseguro, V.; Rodríguez-Hernández, P.; Lavin, V.; Manjón, F. J.; Muñoz, A. Electronic and Elastic Properties of Yttrium Gallium Garnet under Pressure from Ab Initio Studies. *J. Appl. Phys.* **2013**, *113*, 183505 1−7..

(12) Hohenberg, P.; Kohn, W. Inhomogeneous Electron Gas. *Phys. Rev.* **1964**, *136*, B864−B871.

(13) Blöchl, P. E. Projector Augmented-Wave Method. *Phys. Rev. B* **1994**, *50*, 17953−17978.

(14) Perdew, J. P.; Ruzsinszky, A.; Csonka, G. I.; Vydrow, O. A.; Scuseria, G. E.; Constantin, L. A.; Zhou, X.; Burke, K. Restoring the Density-Gradient Expansion for Exchange in Solids and Surfaces. *Phys. Rev. Lett.* **2008**, *100*, 136406 1−4..

(15) Mujica, A.; Rubio, A.; Muñoz, A.; Needs, R. J. High-Pressure Phases of Group-IV, III−V, and II−VI Compounds. *Rev. Mod. Phys.* **2003**, *75*, 863−912.

(16) Parlinsky, K. Computer Code *PHONON*. http://wolf.ifj.edu.pl/phonon.

(17) Yu, F.; Yuan, D.; Cheng, X.; Duan, X.; Wang, X.; Kong, L.; Wang, L.; Li, Z. Preparation and Characterization of Yttrium Gallium Garnet Nanoparticles by Citrate Sol−Gel Method at Low Temperature. *Mater. Lett.* **2007**, *61*, 2322−2324.

(18) Venkatramu, V.; León Luis, S. F.; Rodríguez-Mendoza, U. R.; Monteseguro, V.; Manjón, F. J.; Lozano-Gorrín, A. D.; Valiente, R.; Navarro-Urrios, D.; Jayasankar, C. K.; Muñoz, A.; Lavín, V. Synthesis, Structure and Luminescence of Er^{3+}-Doped $Y_3Ga_5O_{12}$ Nano-Garnets. *J. Mater. Chem.* **2012**, *22*, 13788−13799.

(19) Ching, W. Y.; Xu, Y.-N. Nonscalability and Nontransferability in the Electronic Properties of the Y-Al-O System. *Phys. Rev. B* **1999**, *59*, 12815−12821.

(20) Errandonea, D.; Meng, Y.; Somayazulu, M.; Häusermann, D. Pressure-Induced $\alpha \rightarrow \omega$ Transition in Titanium Metal: a Systematic Study of the Effects of Uniaxial Stress. *Physica B* **2005**, *355*, 116−125.

(21) Mao, H. K.; Xu, J.; Bell, P. M. Calibration of the Ruby Pressure Gauge to 800 kbar under Quasi-Hydrostatic Conditions. *J. Geophys. Res.* **1986**, *91*, 4673−4676.

(22) Klotz, S.; Chervin, J.-C.; Munsch, P.; Le Marchand, G. J. Hydrostatic Limits of 11 Pressure Transmitting Media. *Phys. D: Appl. Phys.* **2009**, *42*, 075413-1−7.

(23) Papagelis, K.; Arvanitidis, J.; Vinga, E.; Christofilos, D.; Kourouklis, G. A.; Kimura, H.; Ves, S. Vibrational Properties of $(Gd_{1-x}Y_x)_3Ga_5O_{12}$ Solid Solutions. *J. Appl. Phys.* **2010**, *107*, 113504 1−8..

(24) Hurrel, J. P.; Porto, S. P. S.; Chang, I. F.; Mitra, S. S.; Bauman, R. P. Optical Phonons of Yttrium Aluminum Garnet. *Phys. Rev.* **1968**, *173*, 851−856.

(25) Moore, R. K.; White, W. B.; Long, T. V. Vibrational Spectra of The Common Silicates: I. The Garnets. *Am. Mineral.* **1971**, *56*, 54−71.

(26) Hofmeister, A. M.; Campbell, K. R. Infrared Spectroscopy of Yttrium Aluminum, Yttrium Gallium, and Yttrium Iron Garnets. *J. Appl. Phys.* **1992**, *72*, 638−646.

(27) Baroni, S.; de Gironcoli, S.; Dal Corso, A.; Giannozzi, P. Phonons and Related Crystal Properties from Density-Functional Perturbation Theory. *Rev. Mod. Phys.* **2001**, *73*, 515−562.

(28) Hua, H.; Mirov, Sergey B.; Vohra, Yogesh K. High-Pressure and High-Temperature Studies on Oxide Garnets. *Phys. Rev. B* **1996**, *54*, 6200−6209.

(29) Birch, F. Finite Elastic Strain of Cubic Crystals. *Phys. Rev.* **1947**, *71*, 809−824.
(30) Milman, V.; Winkler, B.; Nobes, R. H.; Akhmatskaya, E. V.; Pickard, C. J.; White, J. A. Garnets: Structure, Compressibility, Dynamics and Disorder. *J. Met.* **2000**, *52*, 22−25.